Ultraslow diffusion and weak ergodicity breaking in right triangular billiards

Junxiang Huang* and Hong Zhao†

Department of Physics and Institute of Theoretical Physics and Astrophysics, Xiamen University, Xiamen 361005, Fujian, China

(Received 18 March 2016; revised manuscript received 20 January 2017; published 10 March 2017)

We investigate the diffusion behavior of a right triangular billiard system by transforming its dynamics to a two-dimensional piecewise map. We find that the diffusion in the momentum space is ultraslow, i.e., the mean squared displacement grows asymptotically as the square of the logarithm of time. The mechanism of the ultraslow diffusion behavior is explained and numerical evidence corroborating our conclusion is provided. The weak ergodicity breaking of the system is also discussed.

DOI: 10.1103/PhysRevE.95.032209

I. INTRODUCTION

Diffusion is one of the most intriguing and important topics in statistical physics. In most cases, the mean squared displacement (MSD) grows asymptotically in the power law of time, i.e.,

$$\sigma_t^2(q) \sim t^{\eta}, \tag{1}$$

and the power law exponent, η, characterizes subdiffusion ($\eta < 1$), normal diffusion ($\eta = 1$), and superdiffusion ($\eta > 1$), respectively [1–5]. There exists, however, also another class of diffusion behavior where the MSD grows logarithmically in time:

$$\sigma_t^2(q) \sim (\ln t)^{\kappa}, \quad \kappa > 0. \tag{2}$$

This class of anomalous diffusion, termed as ultraslow diffusion or strongly anomalous diffusion, has been found in more and more cases, including the Sinai model ($\kappa = 4$) [6], random motions of a particle in charged polymers [7–9] or aperiodic environments [10,11], a certain family of iterated maps [12], a parabolic map [13], and a non-Markovian random walking [14]. In the continuous-time random walk theory, such ultraslow diffusion has been explained by the waiting time distribution [15].

In this paper we show that the ultraslow diffusion also happens in a generic right triangular billiard system (RTBS). As the simplest one of polygonal billiard systems [16,17], the RTBS is particularly interesting due to its equivalence to the system of two elastic point masses confined to move in a one-dimensional box [18]. Perhaps the most important property of this system lies in the discreteness of its momentum space, which is at the root of many other properties. For example, it is generally acknowledged that if the acute angles of the right triangle are rational multiples of π then the billiard flow is nonergodic. This nonergodicity property is actually a consequence of the momentum discreteness. In view of this, in the following we will first build a full description of the momentum discreteness; then, with the help of this description, we will show that the momentum discreteness is necessary but insufficient for the ultraslow diffusion.

The remainder of this paper is organized as follows. We will first introduce the model and notations in Sec. II. Then in Sec. III, we build a quantitative description of the discretized momenta, and show the ultraslow diffusion in the momentum space. In Sec. IV, we explain the mechanism leading to the ultraslow diffusion. We will also show that if we invalidate the mechanism by perturbing the system, subdiffusion emerges instead. After that, we will address the weak ergodicity breaking problem by studying the disparity between ensemble and time averages in Sec. V. Finally, we will conclude our paper in Sec. VI.

II. THE MODEL

A RTBS describes the motion of a particle confined to move freely in a right triangle. When the particle hits the three sides, it will be reflected back elastically. The only system parameter is one acute angle of the right triangle, denoted as α ($0 < \alpha < \pi/2$). Due to singularities in the billiard flow, the phase trajectories are discontinuous. Based on our understanding of this fact, we transform the dynamics of the RTBS into a two-dimensional piecewise map on the ϑ-x plane, where $\vartheta \in (-\infty, \infty)$ represents the momentum direction of the particle, and $x \in [0, 1]$ represents the position of the particle. Leaving details of this transformation for Appendix A, here we directly give the forward iteration of the map that consists of three pieces:

$$\mathbf{L}: \begin{cases} \vartheta_{i+1} = \lambda - \dfrac{1}{\vartheta_i}, \\ x_{i+1} = -\dfrac{x_i}{\vartheta_i} + \dfrac{1}{\vartheta_i} + 1, \end{cases} \tag{3a}$$

for $\vartheta_i < 0, x_i > 1 + \vartheta_i$;

$$\mathbf{M}: \begin{cases} \vartheta_{i+1} = \lambda - \vartheta_i, \\ x_{i+1} = 1 + \vartheta_i - x_i, \end{cases} \tag{3b}$$

for $-1 \leqslant \vartheta_i \leqslant 1, \vartheta_i \leqslant x_i \leqslant 1 + \vartheta_i$; and

$$\mathbf{R}: \begin{cases} \vartheta_{i+1} = \lambda - \dfrac{1}{\vartheta_i}, \\ x_{i+1} = \dfrac{x_i}{\vartheta_i}, \end{cases} \tag{3c}$$

for $\vartheta_i > 0, x_i < \vartheta_i$.

Here $\lambda \equiv 2\cos 2\alpha \in (-2, 2)$, and the bold-type letters, **L**, **M**, and **R**, represent, respectively, the mapping operation of each piece. As shown in Fig. 1, the ϑ-x plane can be

*jxhuangphys@gmail.com
†zhaoh@xmu.edu.cn

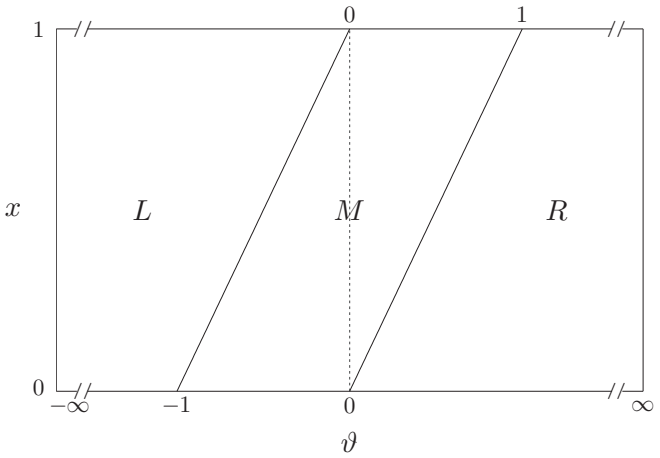

FIG. 1. The forward regions of the forward iteration Eq. (3). The three regions, L, M, and R, are partitioned by the two solid lines the slopes of which equal to 1.

partitioned into three regions, denoted as L, M, and R, that correspond to **L**, **M**, and **R**, respectively. We call these three regions the "forward regions." To map a phase point to its next image, one takes the mapping operation depending on which forward region this phase point belongs to. By mapping a phase point forward repeatedly, we can obtain a forward symbolic sequence made of letters L, M, and R, representing the regions its images visit subsequently. A typical forward sequence is written as $P_1P_2P_3\cdots$, where P_i takes one letter of L, M, and R [19]. A phase point that corresponds to this sequence belongs to region P_1 and will be mapped into region P_2 by $\mathbf{P_1}$ operation, and so on. Note that usually there is an inclined line segment, rather than a single point, that corresponds to a given infinite-long forward symbolic sequence. This means generally every point on a vertical line corresponds to a different infinite-long sequence.

The dynamics of a billiard system is reversible. As a consequence, the equivalent map representation of RTBS, Eq. (3), is also reversible. The corresponding backward iteration formulas are given in Appendix B.

III. ULTRASLOW DIFFUSION

In this section we investigate the diffusion behavior of the map given by Eq. (3). To this end we first define a function $\widetilde{n}$. According to Eqs. (3a) and (3c), the ϑ parts of **L** and **R** operations have the same form. Thus, we use a letter S to represent an L or R. This representation allows us to define a function $\widetilde{n}$ of a symbolic sequence $P_1P_2P_3\cdots P_t$ as follows. First, we replace every L and R in the sequence by S (with M remaining unchanged). Second, suppose that there are n_M letters of M in the given sequence, then denote the total number of S between the ith M and the $(i+1)$th M as n_{even} (n_{odd}), where i is an even (odd) integer and runs from zero (one) to n_M-2 or n_M-1. Third, $\widetilde{n}$ is defined as $\widetilde{n}\equiv n_{\text{even}}-n_{\text{odd}}$. For example, $\widetilde{n}(SSMSM)=1$, and $\widetilde{n}(MSSSM)=-3$.

The function $\widetilde{n}$ is very important. Given an initial point (ϑ_0, x_0) that corresponds to sequence $P_1P_2P_3\cdots P_t$, then ϑ_t, the ϑ variable of the tth image, is totally determined by ϑ_0 and $\widetilde{n}$ of the sequence. In addition, ϑ_0 and $\widetilde{n}$ also determine $\gamma_t\equiv\lim_{|dx_0|\to 0} dx_t/dx_0$, the stretch rate in the x direction. With some calculations (see Appendix C), it can be shown that

$$\begin{aligned}
&\vartheta_t=\Theta^+(\vartheta_0,\widetilde{n}),\gamma_t=\Gamma^+(\vartheta_0,\widetilde{n}),\\
&\qquad\text{if } P_1\cdots P_t \text{ contains an even number of } M;\\
&\vartheta_t=\Theta^-(\vartheta_0,\widetilde{n}),\gamma_t=\Gamma^-(\vartheta_0,\widetilde{n})\\
&\qquad\text{if } P_1\cdots P_t \text{ contains an odd number of } M;
\end{aligned}\tag{4}$$

where

$$\Theta^\pm(\vartheta_0,\widetilde{n})=\frac{\lambda}{2}\pm\frac{\sqrt{4-\lambda^2}}{2}\cot(2\widetilde{n}\alpha+\psi),\tag{5a}$$

$$\Gamma^\pm(\vartheta_0,\widetilde{n})=\pm\frac{\sin\psi}{|\sin(2\widetilde{n}\alpha+\psi)|},\tag{5b}$$

$$\psi=\arcsin\left(\frac{1}{2}\sqrt{\frac{4-\lambda^2}{\vartheta_0^2-\lambda\vartheta_0+1}}\right).\tag{5c}$$

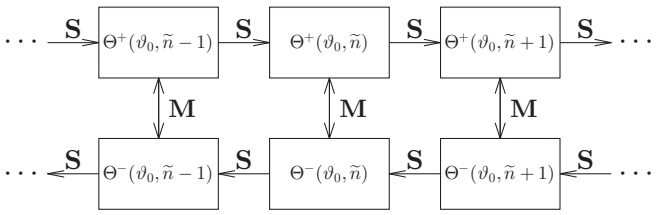

FIG. 2. The evolution diagram of the variable ϑ follows Eqs. (4) and (5a).

According to Eqs. (4) and (5a), the evolution of ϑ can be seen as on a network shown in Fig. 2. The evolution rule is the following: given $\vartheta_i=\Theta^\pm(\vartheta_0,\widetilde{n})$, if P_{i+1} is L or R (represented by S), then ϑ_{i+1} will be $\Theta^\pm(\vartheta_0,\widetilde{n}\pm 1)$; otherwise, P_{i+1} is M, and ϑ_{i+1} will be $\Theta^\mp(\vartheta_0,\widetilde{n})$. This network has several properties that are independent of α. First, two S letters that aligned vertically must be the same. This is because $\Theta^+(\vartheta_0,\widetilde{n})=1/\Theta^-(\vartheta_0,\widetilde{n}+1)$ for an arbitrary $\widetilde{n}$, so the two S between $\widetilde{n}$ and $\widetilde{n}+1$ are both L or both R. This implies that sequences such as LMR or RML are forbidden. Second, half of the vertical arrows, corresponding to **M** operations do not actually exist. Due to the same equation mentioned above, either $|\Theta^+(\vartheta_0,\widetilde{n})|$ or $|\Theta^-(\vartheta_0,\widetilde{n}+1)|$ is bigger than 1. Points with $|\vartheta|>1$ must not belong to the M region (see Fig. 1), so the corresponding vertical M arrows do not exist. Third, all of the horizontal arrows, which correspond to **S** operations, must exist except where $\vartheta=0$. This is because any vertical line segment on the phase plane with $\vartheta\neq 0$ does not totally belong to the M region. These properties limit the construction of the network and the allowed sequences.

It is important to note that for the following three cases the network shown in Fig. 2 can be "folded": (i) if α/π is rational, then both Θ^+ and Θ^- are periodic functions of $\widetilde{n}$; (ii) if $\Theta^\pm(\vartheta_0,\widetilde{n})=\lambda/2$, then $\Theta^+(\vartheta_0,\widetilde{n})=\Theta^-(\vartheta_0,\widetilde{n})$; (iii) if $|\Theta^\pm(\vartheta_0,\widetilde{n})|=1$, then $\Theta^\pm(\vartheta_0,\widetilde{n})=\Theta^\mp(\vartheta_0,\widetilde{n}\pm 1)$. In cases (ii) and (iii), almost all of the trajectories are periodic [20]. Therefore, in all these cases, only a finite number of ϑ values can be reached, and the diffusion behavior of ϑ is stationary,

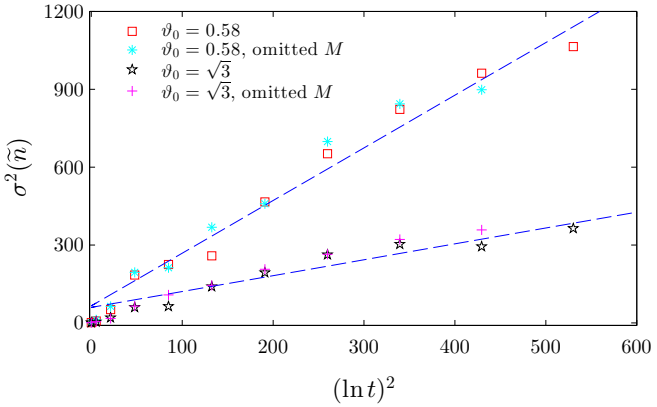

FIG. 3. The dependence of $\sigma^2(\widetilde{n})$ on $(\ln t)^2$. The average ensemble consists of 10^6 initial conditions with identical ϑ_0 but uniformly distributed random x_0. To explore the role of waiting time, another time scale, t_S, by omitting the time of all **M** operations, is also considered.

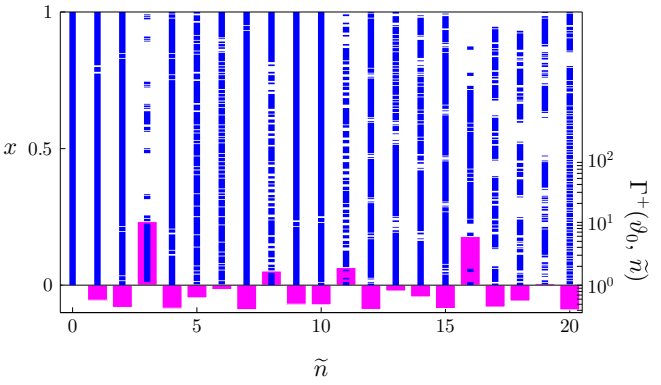

FIG. 4. The first 10^{10} images of the initial point $(\sqrt{3}, 0.5)$ on $\Theta^+(\vartheta_0, \widetilde{n})$, $0 \leqslant \widetilde{n} \leqslant 20$. The temporarily forbidden zones can be seen clearly even for $\widetilde{n} = 3$. The pink bar below is the corresponding $\Gamma^+(\vartheta_0, \widetilde{n})$ plotted for reference.

i.e., strict localization. But once

$$\begin{aligned} &\alpha/\pi \text{ is irrational,} \\ &\vartheta \neq \lambda/2, \pm 1, \end{aligned} \tag{6}$$

the values of $\Theta^{\pm}(\vartheta_0, \widetilde{n})$ are different from each other. It is straightforward to show that the number of different ϑ values visited by a trajectory up to t iterations is always equal to $2K$, where $K = \widetilde{n}_{\max} - \widetilde{n}_{\min} + 1$ is the different $\widetilde{n}$ values the forward sequence can take. Obviously, $\widetilde{n}$ better reflects the "spread distance" between ϑ_t and ϑ_0 than $\vartheta_t - \vartheta_t$ does. In other words, $\sigma^2(\widetilde{n})$ better reflects the diffusion behavior in the ϑ space than $\sigma^2(\vartheta)$ does. We thus will focus on the former in the following.

Before proceeding further, let us first perform a numerical study of the diffusion. We fix $\alpha = (\sqrt{5} - 1)\pi/4$ for all numerical experiments in the following, but note that practically the results do not depend on this particular value [21]. We computer the MSD of $\widetilde{n}$ obtained by evolving an ensemble of trajectories with the same ϑ_0 but random $x_0 \in [0, 1]$. The results are shown in Fig. 3. Despite fluctuations, it can be seen that

$$\sigma_t^2(\widetilde{n}) \sim (\ln t)^2. \tag{7}$$

Note that though at every step a trajectory changes its ϑ value, the $\widetilde{n}$ value stays unchanged under an **M** operation. So k consecutive **M** operations result in an effective waiting time of k steps between two changes in $\widetilde{n}$. One may thus wonder if the observed ultraslow diffusion is caused by this waiting time, like in some other cases of ultraslow diffusion [7–9,12,14,15]. To test this, we omit all **M** operations when counting the time and denote the new time t_S. However, it turns out that $\sigma_{t_S}^2(\widetilde{n})$ depends on $(\ln t_S)^2$ as well, as shown in Fig. 3. In addition, due to the fluctuations, sometimes the MSD at t_S is smaller than that at $t = t_S$, even though the symbolic sequences t_S corresponds to are longer. Therefore, we can safely exclude the possibility that the ultraslow diffusion is caused by this time-delay effect.

IV. THE MECHANISM

Now we turn to the underlying mechanism of the ultraslow diffusion. According to Eqs. (3) and (5b), if a point (ϑ_0, x_0) is mapped to (ϑ_0, x) following a symbolic sequence, then $\Delta x \equiv x - x_0$ can be written as

$$\Delta x = \left(\sum_{i=0}^{|\widetilde{n}|_{\max}} a_i \lambda^i \right) \vartheta_0 + \left(\sum_{j=0}^{|\widetilde{n}-1|_{\max}} b_j \lambda^j \right), \tag{8}$$

where the coefficients a_i and b_j are integers decided by the sequence. For example, $\mathbf{MM}x_0 = x_0 + (-2)\vartheta_0 + (\lambda)$, $\mathbf{MRMR}x_0 = x_0 + (-\lambda - 2)\vartheta_0 + (\lambda^2 + \lambda - 2)$. The sequence must satisfy a series of requirements. For example, to make sure $\vartheta_t = \vartheta_0$, the sequence must contain an even number of M, make $\widetilde{n} = 0$, cannot violate the properties discussed in the last section, and so on. These requirements exclude a big fraction of sequences, and can be transformed to the limitations on Δx.

In stead of explicitly listing all these limitations, we show their overall result in Fig. 4. For a fixed range of visited $\widetilde{n}$, there are gaps between the allowed Δx values. Consequently, some continuous zones in the x direction on the vertical lines are unreachable until the range of visited $\widetilde{n}$ is expanded. This effect is enhanced by big $\Gamma^+(\vartheta_0, \widetilde{n})$ value, and can be clearly seen.

These "temporarily forbidden zones" in turn forbid corresponding sequences, some of which may lead to new $\widetilde{n}$ values. Namely, the Δx values and the sequences limit each other and slow down the diffusion in the $\widetilde{n}$ space. On the other hand, a new reached $\widetilde{n}$ value brings additional Δx, implying some new allowed sequences. These new sequences may lead to more new $\widetilde{n}$ values and cause further increases. Thus, K, the number of all reached $\widetilde{n}$, always exhibits rapid jumps and long plateaus, as shown in Fig. 5. Statistically, K increases as $K \sim \ln t$, which implies an ultraslow diffusion process.

The analysis above indicates that the ultraslow diffusion stems from the existence of temporarily forbidden zones, which partially result from the discreteness of the ϑ space. To test this conclusion, we consider here a counterexample. We break the limitations on Δx by perturbing the evolution of the system: if $\vartheta_{i+1} > 1$ (so that it belongs to the R region) and

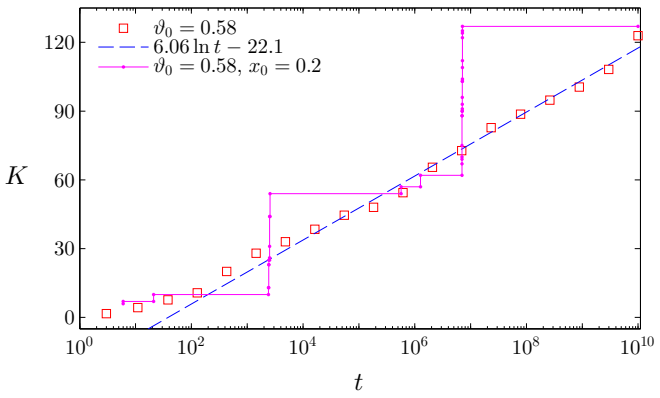

FIG. 5. The time dependence of K, the number of different $\widetilde{n}$ values visited by a trajectory. The squares are for the averaged results over an ensemble of 10^6 initial conditions uniformly distributed along the line $\vartheta_0 = 0.58$. The solid curve is for the result of a single trajectory with initial point $(\vartheta_0, x_0) = (0.58, 0.2)$, as an example. The dashed line is plotted for reference.

$x_{i+1} < 2\varepsilon$, then x_{i+1} is replaced by

$$x'_{i+1} = \begin{cases} x_{i+1} - \varepsilon, & 0 \leqslant x_{i+1} < \varepsilon; \\ x_{i+1} + \varepsilon, & \varepsilon \leqslant x_{i+1} < 2\varepsilon. \end{cases} \tag{9}$$

Here $0 \leqslant \varepsilon \leqslant 1/2$ is an introduced parameter that controls the perturbation: the smaller is ε, the smaller is the perturbation. With the added perturbation, most properties of the system remain unchanged. In particular, the map is still deterministic and reversible, the phase point stays in the R region, and the ϑ space remains discretized. But since Eq. (8) is invalid, the temporarily forbidden zones disappear. Meanwhile, the diffusive behavior changes from the ultraslow diffusion to subdiffusion $\sigma^2(\widetilde{n}) \sim t^\eta$, where the exponent η depends on ε asymptotically as $\eta \sim \varepsilon^{0.13}$ for $\vartheta_0 = \sqrt{3}$ and $10^{-6} \leqslant \varepsilon \leqslant 1/2$, as shown in Fig. 6. The increase of η with ε mainly results from the increase of the perturbation frequency rather than the switch distance. This result is consistent with our finding

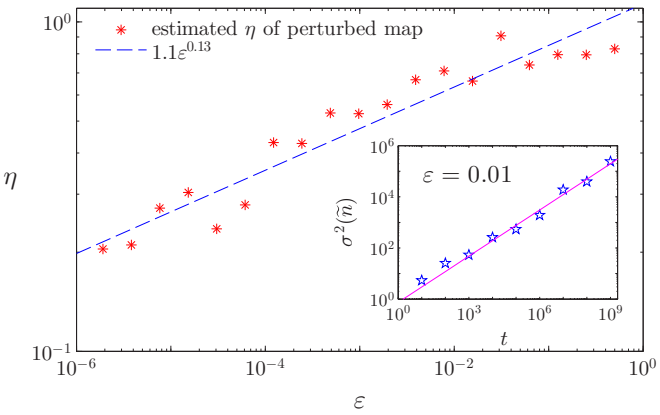

FIG. 6. The dependence of η on ε. The asterisks are for the averaged results over an ensemble of 10^6 initial conditions uniformly distributed along the line $\vartheta_0 = \sqrt{3}$. The dashed line is plotted for reference. In the inset we show the time dependence of $\sigma^2(\widetilde{n})$ for $\varepsilon = 0.01$ as an example. The solid line gives the slope $\eta = 0.6$.

that the ultraslow diffusion stems from the mutual limitations between Δx values and the forward sequences.

V. WEAK ERGODICITY BREAKING

The RTBS is equivalent to the system of two hard particles colliding with each other and the walls in a one-dimensional box [22]. Some authors have investigated the ergodic properties of the billiard flow in an irrational RTBS or in the equivalent two-colliding-particle model. In Ref. [23], it is stated that the irrational RTBS is ergodic and weakly mixing. In Ref. [24], it is suggested that the two-colliding-particle model with an irrational parameter is ergodic and mixing. It is worth mentioning that Vorobets has proved that with some kind of weak irrational α/π, the RTBS flow is ergodic, in the sense that the phase spaces cannot be subdivided into mutually inaccessible regions [25]. On the other hand, recently there is some numerical evidence suggesting localization in the two-colliding-particle model, implying that with a strongly irrational system parameter the model may be nonergodic [26,27].

In Sec. IV, we have shown that limited $\widetilde{n}$ range gives rise to the vertical forbidden zones, which will gradually become reachable when new $\widetilde{n}$ values appear. Otherwise, it is easy to show that if these forbidden zones exist permanently they will lead to broken ergodicity of the system. Our numerical experiments suggest that the localization effect reported in [26,27] should be due to the ultraslow diffusion, which is not necessarily related to the subdivision of the phase space. Therefore, whether a generic irrational RTBS is ergodic still needs an analytic study.

In stead of strict ergodicity, here we address the weak ergodicity breaking in the model, i.e., the disparity between averages over time and over the phase space at any meaningful time scale [28–30]. This disparity includes two parts. First, the average time needed to increase a fixed amount of $\sigma^2(\widetilde{n})$ diverges rapidly. Compared with a power-law diffusion process, the fraction of the visited ϑ values up to time t is negligibly small, of order $(\ln t)/t^{\eta/2}$, as $t \to \infty$. Second, the ultraslow diffusion in the ϑ space implies that on some ϑ values there remain continuous unreachable segments of x, thanks to the limitations on Δx values. This weak ergodicity breaking is compatible with previous results that the system is ergodic with certain parameter values [25].

VI. CONCLUSION

We have shown the ultraslow diffusion in the $\widetilde{n}$ space of a right triangular billiard system, where $\widetilde{n}$ has a clear physical meaning related to the discreteness of the variable ϑ. This ultraslow diffusion, shown to stem from the temporary existences of forbidden zones, cannot be ascribed to the waiting time between two consecutive changes in $\widetilde{n}$. In addition, destroying the forbidden zones by perturbations gives rise to subdiffusion. These facts also shed a light on the study of the ergodic properties.

As the model is extremely simple in construction, it may provide basic understanding to other complex models, e.g., polygonal billiards and hard-core gases. In addition, its dynamical behavior is very similar to the so-called generalized triangle map with special parameters. In such a map, similar

discreteness of the phase space and ultraslow diffusion are also observed [31]. Furthermore, the RTBS has been studied for decades mainly by using the geodesic methods [32–34]. Since the equivalent map defined by Eq. (3) is much easier to manipulate than the geodesic methods in some aspects, this advantage may be useful for extending our method to study other nonlinear systems.

ACKNOWLEDGMENT

This work is supported by NSFC (Grant No. 11335006).

APPENDIX A: DERIVATION OF EQ. (3)

To describe the state of the particle at an arbitrary moment, i.e., to pin down a point in the whole phase space, we need three variables: two represent its position and one represents its momentum direction. The speed is a constant because all collisions are elastic. However, if we focus on the instants the particle collides with the hypotenuse, the two position variables collapse to one variable x, i.e., the location where the particle collides with the hypotenuse. We fix the length of the hypotenuse to be unity and set the α vertex point to be the origin, then we have $x \in [0, 1]$. The variable represents that the momentum direction is the rebound angle, denoted as $\theta \in (0, \pi)$, as shown in Fig. 7. In summary, we use two variables θ and x to represent a Poincaré section of the phase space.

What we need now is the evolution rules on the Poincaré section. Between two consecutive collisions with the hypotenuse, there are three possible events. If we fix the x_i value and vary θ_i from zero to 2π, these events will appear in the following order: (1) one collision with only the opposite side of α, (2) two collisions with both legs, and (3) one collision with only the adjacent side of α. Motivated by this fact, we separate the motion of the particle at every instant right after it collides with the hypotenuse, and denote the combination of the hypotenuse collision and the followed event by L, M, and R, respectively. In other words, every letter represents one collision with the hypotenuse plus one or two collisions with the legs. For example, as illustrated in Fig. 7, a letter R represents that the motion starts from the instant right after the particle collides with the hypotenuse, through a collision with the adjacent side of α, to the next collision with the hypotenuse.

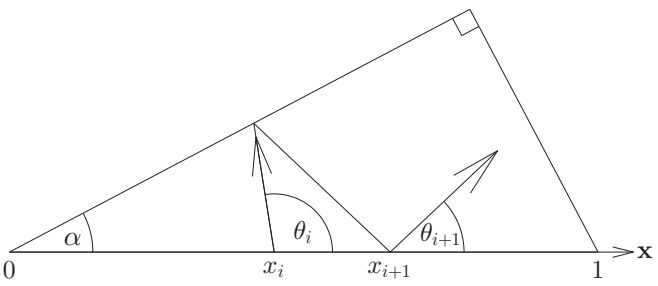

FIG. 7. A particle moves in a right triangular billiard the hypotenuse of which has unit length. The collisions between the particle and the sides are all elastic. The motion in the figure from leaving x_i to colliding with the hypotenuse at x_{i+1} is denoted by a letter R, the mapping formula of which for θ and x can be derived using the law of sines.

Based on the angular relation of elastic collisions and the law of sines, the conditions and formulas of forward iteration can be written in terms of θ and x as

$$\mathbf{L}: \begin{cases} \theta_{i+1} = \theta_i - 2\alpha + \pi, \\ x_{i+1} = (1 - x_i)\dfrac{\sin\theta_i}{\sin(\theta_i - 2\alpha)} + 1, \end{cases} \tag{A1a}$$

for $0 < \theta_i < 2\alpha$, $x_i > 1 + \frac{\sin(\theta_i - 2\alpha)}{\sin\theta_i}$;

$$\mathbf{M}: \begin{cases} \theta_{i+1} = \pi - \theta_i, \\ x_{i+1} = 1 + \dfrac{\sin(\theta_i - 2\alpha)}{\sin\theta_i} - x_i, \end{cases} \tag{A1b}$$

for $\alpha \leqslant \theta_i \leqslant \pi/2 + \alpha$, $\frac{\sin(\theta_i - 2\alpha)}{\sin\theta_i} \leqslant x_i \leqslant 1 + \frac{\sin(\theta_i - 2\alpha)}{\sin\theta_i}$; and

$$\mathbf{R}: \begin{cases} \theta_{i+1} = \theta_i - 2\alpha, \\ x_{i+1} = x_i \dfrac{\sin\theta_i}{\sin(\theta_i - 2\alpha)}, \end{cases} \tag{A1c}$$

for $2\alpha \leqslant \theta_i < \pi$, $x_i < \frac{\sin(\theta_i - 2\alpha)}{\sin\theta_i}$.

To simplify the expressions, we replace θ with

$$\vartheta = \frac{\sin(\theta - 2\alpha)}{\sin\theta} \in (-\infty, \infty), \tag{A2}$$

and α with $\lambda = 2\cos 2\alpha$. What we obtain is Eq. (3).

APPENDIX B: THE BACKWARD ITERATION FORMULAS OF THE MAP

The corresponding backward iteration can be directly derived from Eq. (3):

$$\mathbf{L}^{-1}: \begin{cases} \vartheta_i = \dfrac{1}{\lambda - \vartheta_{i+1}}, \\ x_i = -\dfrac{x_{i+1}}{\lambda - \vartheta_{i+1}} + \dfrac{1}{\lambda - \vartheta_{i+1}} + 1, \end{cases} \tag{B1a}$$

for $\vartheta_{i+1} > \lambda$, $x_{i+1} > 1 + \lambda - \vartheta_{i+1}$;

$$\mathbf{M}^{-1}: \begin{cases} \vartheta_i = \lambda - \vartheta_{i+1}, \\ x_i = 1 + \lambda - \vartheta_{i+1} - x_{i+1}, \end{cases} \tag{B1b}$$

for $\lambda - 1 \leqslant \vartheta_{i+1} \leqslant \lambda + 1$, $\lambda - \vartheta_{i+1} \leqslant x_{i+1} \leqslant 1 + \lambda - x_{i+1}$; and

$$\mathbf{R}^{-1}: \begin{cases} \vartheta_i = \dfrac{1}{\lambda - \vartheta_{i+1}}, \\ x_i = \dfrac{x_{i+1}}{\lambda - \vartheta_{i+1}}, \end{cases} \tag{B1c}$$

for $\vartheta_{i+1} < \lambda$, $x_{i+1} < \lambda - \vartheta_{i+1}$.

Likewise, we can partition the phase plane into three backward regions which correspond to $\mathbf{L}^{-1}$, $\mathbf{M}^{-1}$, and $\mathbf{R}^{-1}$, respectively. It is easy to see that the forward and backward regions, as well as the forward and backward iterations, are symmetric with respect to the line $\vartheta = \lambda/2$.

APPENDIX C: DERIVATIONS OF EQS. (4) AND (5)

For the sake of convenience, if a sequence contains an even number of M, we call it an even sequence; otherwise we call

it an odd sequence. We represent calculation for only even sequences here. The results for odd sequences are given at the end of the section. First, let us focus on ϑ_t, and omit the evolution of the x variable. Since we can calculate ϑ_t according to ϑ_0 and the sequence $P_1 \cdots P_t$, it is convenient to use $\vartheta_t = \mathbf{P_1} \cdots \mathbf{P_t}\vartheta_0$ to record this relation, where ϑ_t is the ϑ value of the tth image of (ϑ_0, x_0). We have

$$\mathbf{SMS}\vartheta = \mathbf{M}\vartheta = \lambda - \vartheta, \quad \mathbf{MM}\vartheta = \vartheta. \tag{C1}$$

Equation (C1) provides two rules, based on which we can calculate whether two sequences lead to the same ϑ value. Surprisingly, we find that the final ϑ value after an even sequence depends only on ϑ_0 and $\widetilde{n}$ of the sequence, i.e., equals to $\mathbf{S}^{\widetilde{n}}\vartheta_0$. Take the sequences mentioned in Sec. III for example. $\mathbf{SSMSM}\vartheta_0 = \mathbf{S}\vartheta_0$, and $\mathbf{MSSSM}\vartheta_0 = \mathbf{S}^{-3}\mathbf{S}^3\mathbf{M}\mathbf{S}^3\mathbf{M}\vartheta_0 = \mathbf{S}^{-3}\vartheta_0$. Therefore, the ϑ_t value, obtained after the initial point follows an even sequence $P_1 \cdots P_t$, is a function of ϑ_0 and $\widetilde{n}$, which can be denoted by

$$\Theta^+(\vartheta_0, \widetilde{n}) = \mathbf{S}^n\vartheta_0, \tag{C2}$$

To find out its expression, we introduce an intermediate array $\{W(\vartheta_0, \widetilde{n}) \mid \widetilde{n} \in \mathbb{Z}\}$ defined by

$$\begin{aligned} W(\vartheta_0, \widetilde{n}+1) &= \Theta^+(\vartheta_0, \widetilde{n})W(\vartheta_0, \widetilde{n}), \\ W(\vartheta_0, 0) &= 1. \end{aligned} \tag{C3}$$

According to Eq. (C2), we have

$$\begin{aligned} \Theta^+(\vartheta_0, \widetilde{n}) &= \mathbf{S}\Theta^+(\vartheta_0, \widetilde{n}-1) \\ &= \lambda - 1/\Theta^+(\vartheta_0, \widetilde{n}-1). \end{aligned} \tag{C4}$$

Using it in Eq. (C3), we get

$$\begin{aligned} W(\vartheta_0, \widetilde{n}+1) &= \left[\lambda - \frac{1}{\Theta^+(\vartheta_0, \widetilde{n}-1)}\right] W(\vartheta_0, \widetilde{n}) \\ &= \lambda W(\vartheta_0, \widetilde{n}) - W(\vartheta_0, \widetilde{n}-1) \\ &= 2\cos(2\alpha)W(\vartheta_0, \widetilde{n}) - W(\vartheta_0, \widetilde{n}-1). \end{aligned} \tag{C5}$$

This equation can be rewritten as

$$\begin{aligned} &W(\vartheta_0, \widetilde{n}+1) - e^{\pm i2\alpha}W(\vartheta_0, \widetilde{n}) \\ &\quad = e^{\mp i2\alpha}[W(\vartheta_0, \widetilde{n}) - e^{\pm i2\alpha}W(\vartheta_0, \widetilde{n}-1)]. \end{aligned} \tag{C6}$$

Since $W(\vartheta_0, 0) = 1$ and $W(\vartheta_0, 1) = \vartheta_0$, it follows that

$$\begin{aligned} W(\vartheta_0, \widetilde{n}) &= \frac{\vartheta_0(e^{i2\widetilde{n}\alpha} - e^{-i2\widetilde{n}\alpha}) - (e^{i2(\widetilde{n}-1)\alpha} - e^{-i2(\widetilde{n}-1)\alpha})}{e^{i2\alpha} - e^{-i2\alpha}} \\ &= \frac{\vartheta_0 \sin(2\widetilde{n}\alpha) - \sin[2(\widetilde{n}-1)\alpha]}{\sin 2\alpha} \\ &= \frac{1}{\sin\psi}\sin(2\widetilde{n}\alpha + \psi), \end{aligned} \tag{C7}$$

where

$$\begin{aligned} \psi &= \arcsin\left(\frac{\sin 2\alpha}{\sqrt{(\vartheta_0 - \cos 2\alpha)^2 + \sin^2 2\alpha}}\right) \\ &= \arcsin\left(\frac{1}{2}\sqrt{\frac{4-\lambda^2}{\vartheta_0^2 - \lambda\vartheta_0 + 1}}\right) \end{aligned} \tag{C8}$$

is a constant for fixed λ and ϑ_0. Combining this expression with Eq. (C3), it follows that

$$\begin{aligned} \Theta^+(\vartheta_0, \widetilde{n}) &= \frac{W(\vartheta_0, \widetilde{n}+1)}{W(\vartheta_0, \widetilde{n})} \\ &= \frac{\sin[2(\widetilde{n}+1)\alpha + \psi]}{\sin(2\widetilde{n}\alpha + \psi)} \\ &= \cos(2\alpha) + \cot(2\widetilde{n}\alpha + \psi)\sin(2\alpha) \\ &= \frac{\lambda}{2} + \frac{\sqrt{4-\lambda^2}}{2}\cot(2\widetilde{n}\alpha + \psi). \end{aligned} \tag{C9}$$

Second, let us turn to the stretch rate in the x direction. Let $x_t = \mathbf{P_1} \cdots \mathbf{P_t}x_0$ be the x value of the tth image after an even sequence $P_1 \cdots P_t$. Though practically ϑ_i is needed to calculate x_{i+1}, here we just omit the ϑ part of the coordinate for convenience, considering that ϑ_i can be derived from ϑ_0 and the sequence. Using such notations, given an infinitesimal perturbation $d(x_0)$, we have

$$\begin{aligned} d(\mathbf{S}x_0) &= \frac{d(x_0)}{|\vartheta_0|}, \\ d(\mathbf{SMS}x_0) &= d(\mathbf{M}x_0) = -d(x_0). \end{aligned} \tag{C10}$$

Here we assume that an infinitesimal perturbation does not change the forward sequence. The second equation is valid thanks to the fact that LMR and RML are forbidden, as we explained in Sec. III. Likewise, the final value of a perturbation $d(x_0)$ after an even sequence depends only on ϑ_0 and $\widetilde{n}$ of the sequence, i.e., equals to $d(\mathbf{S}^n x_0)$. For example, $d(\mathbf{SSMSM}x_0) = d(\mathbf{S}x_0)$, and $d(\mathbf{MSSSM}x_0) = d(\mathbf{S}^{-3}x_0)$. This result implies a stretch rate in the x direction as a function of ϑ_0 and $\widetilde{n}$, which can be denoted by

$$\Gamma^+(\vartheta_0, \widetilde{n}) = \frac{d(\mathbf{S}^n x_0)}{d(x_0)}. \tag{C11}$$

Using Eq. (C10) here, we have

$$\begin{aligned} \Gamma^+(\vartheta_0, \widetilde{n}) &= \frac{\Gamma^+(\vartheta_0, \widetilde{n}-1)}{|\Theta^+(\vartheta_0, \widetilde{n}-1)|} \\ &= \left|\frac{W(\vartheta_0, \widetilde{n}-1)}{W(\vartheta_0, \widetilde{n})}\right| \Gamma^+(\vartheta_0, \widetilde{n}-1) \\ &= \left|\frac{W(\vartheta_0, \widetilde{n}-1)}{W(\vartheta_0, \widetilde{n})} \cdots \frac{W(\vartheta_0, 0)}{W(\vartheta_0, 1)}\right| \Gamma^+(\vartheta_0, 0) \\ &= \frac{1}{|W(\vartheta_0, \widetilde{n})|} = \frac{\sin\psi}{|\sin(2\widetilde{n}\alpha + \psi)|}. \end{aligned} \tag{C12}$$

Γ^+ is always bigger than zero, which means an even sequence keeps the order in the x direction if the points follow the same sequence. In addition, when a line segment $[x_0, x_0 + dx]$ on $\vartheta = \vartheta_0$ is mapped to $\Theta^+(\vartheta_0, \widetilde{n})$, even if the points follow different sequences, the total length of the images (every point counts once) is always $\Gamma^+(\vartheta_0, \widetilde{n})dx$.

The cases of odd sequences can be calculated similarly. In such cases, the ϑ value of the tth image is $\Theta^-(\vartheta_0, \widetilde{n}) = \lambda - \Theta^+(\vartheta_0, \widetilde{n})$, and the stretch rate in the x direction is $\Gamma^-(\vartheta_0, \widetilde{n}) = -\Gamma^+(\vartheta_0, \widetilde{n})$. Combining the results for both kinds of sequences, we obtain Eqs. (4) and (5).

[1] R. Metzler and J. Klafter, J. Phys. A **37**, R161 (2004).
[2] J. Klafter and I. M. Sokolov, Phys. World **18**, 29 (2005).
[3] A. Piryatinska, A. I. Saichev, and W. A. Woyczynski, Physica A **349**, 375 (2005).
[4] R. Metzler, J. H. Jeon, A. G. Cherstvy, and E. Barkai, Phys. Chem. Chem. Phys. **16**, 24128 (2014).
[5] V. Zaburdaev, S. Denisov, and J. Klafter, Rev. Mod. Phys. **87**, 483 (2015).
[6] Y. Sinai, Theory Probab. Appl. **27**, 256 (1982).
[7] S. Havlin, A. Bunde, Y. Glaser, and H. E. Stanley, Phys. Rev. A **34**, 3492 (1986).
[8] D. Cassi and S. Regina, Phys. Rev. Lett. **76**, 2914 (1996).
[9] O. Benichou and G. Oshanin, Phys. Rev. E **66**, 031101 (2002).
[10] F. Igloi, L. Turban, and H. Rieger, Phys. Rev. E **59**, 1465 (1999).
[11] S. Arias, X. Waintal, and J. L. Pichard, Eur. Phys. J. B **10**, 149 (1999).
[12] J. Drager and J. Klafter, Phys. Rev. Lett. **84**, 5998 (2000).
[13] T. Prosen and M. Znidaric, Phys. Rev. Lett. **87**, 114101 (2001).
[14] M. A. A. da Silva, G. M. Viswanathan, and J. C. Cressoni, Phys. Rev. E **89**, 052110 (2014).
[15] S. Havlin and G. H. Weiss, J. Stat. Phys. **58**, 1267 (1990).
[16] E. Gutkin, J. Stat. Phys. **83**, 7 (1996).
[17] E. Gutkin, Chaos **22**, 026116 (2012).
[18] S. L. Glashow and L. Mittag, J. Stat. Phys. **87**, 937 (1997).
[19] B. Hao and W. Zheng, *Applied Symbolic Dynamics and Chaos* (World Scientific, Singapore, 1998).
[20] B. Cipra, R. M. Hanson, and A. Kolan, Phys. Rev. E **52**, 2066 (1995).
[21] Actually, the results can be applied to even rational $\alpha/\pi = p/q$ for small t, and the applicable time scale increases exponentially with q while α is limited in a narrow range.
[22] I. P. Cornfeld, S. V. Fomin, and Y. G. Sinai, *Ergodic Theory* (Springer, Berlin, 2012).
[23] R. Artuso, G. Casati, and I. Guarneri, Phys. Rev. E **55**, 6384 (1997).
[24] G. Casati and J. Ford, J. Comput. Phys. **20**, 97 (1976).
[25] Y. B. Vorobets, Sb. Math. **188**, 389 (1997).
[26] M. Hasegawa, Phys. Lett. A **242**, 19 (1998).
[27] J. Wang, G. Casati, and T. Prosen, Phys. Rev. E **89**, 042918 (2014).
[28] M. Thaler, Ergo. Th. Dynam. Syst. **22**, 1289 (2002).
[29] G. Bel and E. Barkai, Europhys. Lett. **74**, 15 (2006).
[30] T. Akimoto, J. Stat. Phys. **132**, 171 (2008).
[31] I. Guarneri, G. Casati, and V. Karle, Phys. Rev. Lett. **113**, 174101 (2014).
[32] G. Galperin and D. Zvonkine, Regul. Chaotic Dyn. **8**, 29 (2003).
[33] S. Troubetzkoy, Ann. Inst. Fourier **55**, 29 (2005).
[34] W. P. Hooper, Geom. Dedic. **125**, 39 (2007).